

UHRF1 is indispensable for meiotic sex chromosome inactivation and interacts with the DNA damage response pathway in mice[†]

Mengneng Xiong^{1,‡}, Shumin Zhou^{1,‡}, Shenglei Feng^{1,‡}, Yiqian Gui¹, Jinmei Li¹, Yanqing Wu¹, Juan Dong¹ and Shuiqiao Yuan^{1,2,3,*}

¹Institute of Reproductive Health, Tongji Medical College, Huazhong University of Science and Technology, Wuhan, China

²Shenzhen Huazhong University of Science and Technology Research Institute, Shenzhen, Guangdong, China

³Laboratory of Animal Center, Huazhong University of Science and Technology, Wuhan, China

*Correspondence: Institute Reproductive Health, Tongji Medical College, Huazhong University of Science and Technology, Wuhan, Hubei 430030, China. Tel: +8615527507840; Fax: +8602783692651; E-mail: shuiqiaoyuan@hust.edu.cn

[†]Grant Support: This work was supported by grants from the National Natural Science Foundation of China (81971444 and 82171605 to SY), the Strategic Collaborative Research Program of the Ferring Institute of Reproductive Medicine, Ferring Pharmaceuticals, and Chinese Academy of Sciences (FIRMSC200502 COV02 to SY), and the Science Technology and Innovation Commission of Shenzhen Municipality (JCYJ20170818160910316 to SY).

[‡]These authors contributed equally to this work.

Abstract

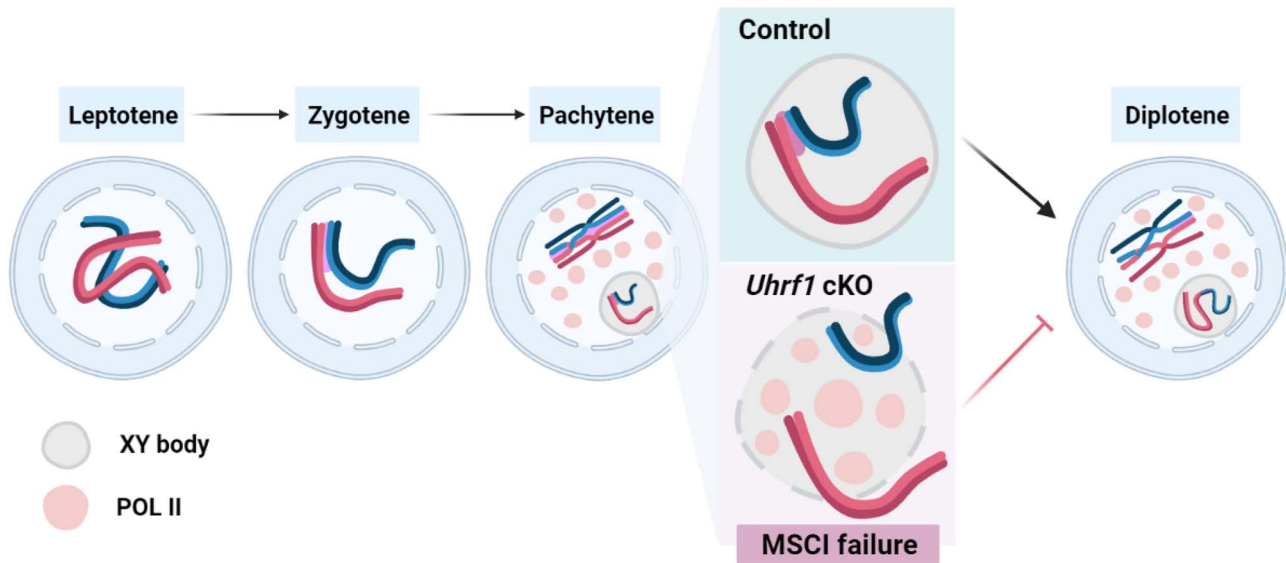
During male meiosis, the constitutively unsynapsed XY chromosomes undergo meiotic sex chromosome inactivation (MSCI), and the DNA damage response (DDR) pathway is critical for MSCI establishment. Our previous study showed that UHRF1 (ubiquitin-like, with PHD and ring finger domains 1) deletion led to meiotic arrest and male infertility; however, the underlying mechanisms of UHRF1 in the regulation of meiosis remain unclear. Here, we report that UHRF1 is required for MSCI and cooperates with the DDR pathway in male meiosis. UHRF1-deficient spermatocytes display aberrant pairing and synapsis of homologous chromosomes during the pachytene stage. In addition, UHRF1 deficiency leads to aberrant recruitment of ATR and FANCD2 on the sex chromosomes and disrupts the diffusion of ATR to the XY chromatin. Furthermore, we show that UHRF1 acts as a cofactor of BRCA1 to facilitate the recruitment of DDR factors onto sex chromosomes for MSCI establishment. Accordingly, deletion of UHRF1 leads to the failure of meiotic silencing on sex chromosomes, resulting in meiotic arrest. In addition to our previous findings, the present study reveals that UHRF1 participates in MSCI, ensuring the progression of male meiosis. This suggests a multifunctional role of UHRF1 in the male germline.

Summary Sentence

UHRF1 is directly interacts with BRCA1 and has critical role in meiotic sex chromosome inactivation (MSCI).

Graphical Abstract

Stages of Meiotic Prophase I



Keywords: DNA damage response, male infertility, meiosis, meiotic sex chromosome inactivation (MSCI), UHRF1

Introduction

Meiosis is a pivotal process for sexual reproduction in which diploid cells divide into haploid cells. During this process, diploid cells proceed through the pre-meiotic S phase and then enter the extended prophase of meiosis I (the leptotene, zygotene, pachytene, diplotene, and diakinesis stages) to reach the first and second meiotic divisions. Multiple specific chromosomal events occur during the prophase of meiosis I, such as chromosome axis formation, homolog recombination, pairing, and synapsis, to allow proper alignment and separation [1]. Homologous recombination is initiated by programmed DNA double-strand breaks (DSBs), which occur at leptotema and induce the linkage and pairing of two individual interacting DNA segments. Following pairing, the axial element extends along the entire length of the chromosome axis, and homologs come closer to each other to form a more robust synaptonemal complex (SC) called synapsis. The stage of SC formation is defined as “zygotene,” and when the formation of SC is completed, the cells enter “pachytene” [2]. At the pachytene stage, all autosomal chromosomes complete pairing and synapsis, but male meiotic X and Y chromosomes are largely heterologous and only partially pair or synapse by their pseudoautosomal regions (PARs) [3].

Defective synapsis is toxic to the meiotic cells and will be eliminated by surveillance mechanisms during the pachytene stage. Increased evidence suggests that asynapsed chromosomes at pachynema undergo meiotic silencing of unsynapsed chromatin (MSUC) [4, 5] in response to unsynapsis [6–8]. Importantly, meiotic silencing of the asynapsed XY chromosome regions at pachynema is essential for male meiosis. Meiotic sex chromosome inactivation (MSCI) is a sex chromosome-specific process for transcriptional silencing of the X and Y chromosomes in the mammalian male germline

[9]. MSCI emerges at the pachytene stage after autosomal homolog pairing and synapsis has been completed, and is mediated by a large-scale chromatin remodeling of the X and Y chromosomes [10]. In addition, MSCI is initiated and directed by the DNA damage response (DDR) pathway, a carefully monitored cellular network that identifies DNA damage and activates DNA damage repair and cell cycle checkpoints to guard genome integrity [11, 12]. In meiosis, DDR proteins function as the “effectors” localized on the unsynapsed axes. Once autosomes have completed synapsis and recombination at the onset of the pachytene stage, DDR proteins are removed from autosomes, and autosomes become transcriptionally active. However, DDR proteins remain in the “XY body” containing partially synapsed sex chromosomes and direct the inactivation of the meiotic sex chromosome. BRCA1, one of the earliest DDR factors involved in XY body formation, binds to unsynapsed axes and recruits ATR to initiate γ H2AX phosphorylation, followed by the MDC1-dependent expansion of γ H2AX to chromatin loops [13, 14]. Evidence has shown that meiotic deficiency of DDR factors causes MSCI defects and meiotic failures, such as *Brca1* [15], *ATR* [16], and *Topbp1* [7]. However, the mechanism by which the DDR pathway triggers the inactive state of the unsynapsed chromosome remains largely unknown.

UHRF1 (Ubiquitin-like, with PHD and RING finger domains 1, also known as NP95 or ICBP90) is a ubiquitin E3 ligase that is best known for its function in DNA methylation and histone modification. This ligase binds to hemi-methylated DNA and tethers DNMT1 to catalyze the methylation of a newly synthesized daughter DNA strand, and has been found to play multiple roles in histone modifications such as H3R2me0, H3K4me0, H3K9me2/3, and H3 ubiquitination [17–20]. Remarkably, previous studies

have indicated that UHRF1 is linked to DDR by cooperating with DDR factors such as the Fanconi anemia (FA) protein FANCD2 during somatic DNA damage repair to protect genome stability [21–24]. In previous studies, including our own, UHRF1 has been reported to repress retrotransposons and links DNA methylation, histone modification, and piRNA pathways by interacting with DNMT1, PRMT5, and PIWI proteins. It has also been found to be essential for spermatogenesis and male fertility [25–27]. The loss of UHRF1 has been reported to result in massive depletion of pachytene spermatocytes during meiotic prophase I, as well as impaired homologous chromosome pairing and synapsis [25–27]. However, the role and molecular mechanism of UHRF1 in male MSCI at the pachytene stage during male meiosis still needs to be elucidated.

In this study, we showed that UHRF1 participates in the MSCI process to ensure the progression of male meiosis using our previously generated *Uhrf1* conditional mouse model. UHRF1-deficient spermatocytes exhibit absent and/or aberrant sex chromosomal pairing, failure of DDR factors recruitment onto sex chromosomes, and disturbed XY body formation, leading to defective MSCI. Mechanistically, we found that UHRF1 is involved in the DDR pathway for the regulation of MSCI by interacting with BRCA1. These results reveal a novel role of UHRF1 in the regulation of male meiotic prophase and provide a potential regulatory mechanism for the MSCI process, which adds another layer of a function of UHRF1 in male germ cell development.

Material and methods

Ethics statement

All animal procedures were approved by the Institutional Animal Care and Use Committee of Tongji Medical College, Huazhong University of Science and Technology, and the mice were housed in the specific pathogen-free facility of Huazhong University of Science and Technology. All experiments with mice were conducted ethically according to the Guide for the Care and Use of Laboratory Animal guidelines.

Generation of *Uhrf1* conditional knockout mice

Uhrf1^{fllox/fllox} mice were generated by embryonic stem cell (ESC) targeting and blastocyst injection at the Shanghai Research Center for Model Organisms as reported previously [25]. *Stra8-Cre* mice in a C57BL/6 J background were purchased from the Jackson Laboratory. *Ngn3-Cre* mice were generously gifted by Prof. Lan Ye at Nanjing Medical University. *Ngn3-Cre* mice were obtained from the Jackson Laboratory (Stock numbers: *Ngn3-Cre*, 06333). *Uhrf1^{fllox/fllox}* mice were crossed with transgenic mice expressing CRE recombinase under the control of the *Stra8* or *Ngn3* promoter to generate *Uhrf1^{fllox/+}* Cre-carrying offspring, which were further crossed with *Uhrf1^{fllox/fllox}* mice to produce *Uhrf1^{fllox/-}*; *Stra8-Cre* or *Uhrf1^{fllox/-}*; *Ngn3-Cre* mice, respectively. Primers used for genotyping for *Uhrf1* floxed and Cre alleles are listed in [Supplementary Table S1](#).

Histology and immunofluorescence

For histology, testes were fixed in Bouin solution (Lot#SLBJ385 5V, Sigma) overnight, dehydrated in ethanol, embedded in paraffin, sectioned, and stained with periodic acid-Schiff (PAS) kit according to the manufacturer's instructions.

Immunofluorescence was performed on frozen sections of testes. Briefly, testes were fixed in 4% paraformaldehyde, dehydrated in sucrose, and embedded in O.C.T (Sakura Finetek, 4583). Five-micrometer-thick cryosections were cut and washed with PBS three times. For antigen retrieval, cryosections were microwaved in 0.01 M sodium citrate buffer (pH = 6.0) and then cooled down to room temperature. After washing with PBS three times (10 min per wash), the sections were blocked in blocking solution (containing 5% normal donkey serum) for 1 h. Tissue sections were then incubated with primary antibodies and secondary antibodies and mounted with DAPI (H1200, Vector Laboratories) and photographed.

Meiotic chromosome spreads assay and immunocytochemistry

Meiotic chromosome spreads were performed as described previously [28]. In brief, the testes were excised, the tunica albuginea was removed, and the seminiferous tubules were separated and washed in ice-cold PBS three times. Next, seminiferous tubules were incubated in hypotonic extraction buffer (50 mM sucrose, 30 mM Tris-base, 17 mM trisodium citrate, 5 mM dithiothreitol (DTT), 5 mM ethylenediaminetetraacetic acid (EDTA), and 1 × complete protease inhibitor cocktail (pH = 8.2) for 1.5–2 h. After this incubation, seminiferous tubules were transferred to a 100 mM sucrose solution and gently mashed with tweezers to release germ cells. Then, approximately 30 μ L of diluted suspension was applied to a positively charged slide that was pretreated with fixation solution (2% paraformaldehyde, 0.02% sodium monododecyl sulfate, 0.05% Triton X-100, and sodium borate buffer to adjust the pH to 9.2). The slides were incubated in humid chambers at RT for 3 h. Then, the slides were washed twice in 0.4% Photo-Flo 200 (Kodak, 146–4 510) for 2 min each. The slides were air-dried at RT for 15–30 min and then blocked with blocking solution (containing 5% normal donkey serum) for 1 h before incubation with primary antibodies. Primary antibodies used for immunofluorescence were as follows: anti-SYCP3 (Santa sc-74569), anti-SYCP1 (Abcam, ab15090), anti-MDC1 (a gift from Dr Mengcheng Luo, Wuhan University, China), anti- γ H2AX (Abcam, ab81299), anti-ATR (Santa, sc-515173), anti-H1T (Proteintech, 18188-1-AP), anti-HORMAD1 (Proteintech, 13917-1-AP), anti-TOPBP1 (Proteintech, 23340-1-AP), anti-BRCA1 (a gift from Dr Linyv Lu, Zhejiang University, China), anti-H3K9me3 (Abclonal, A2360), anti-CREST (Antibodies Incorporated, 15-234-0001), anti-UHRF1 (Santa, sc-373750), anti-H3K9ac (Abclonal, A7255), anti-FANCD2 (Boster, BM4604), anti-ATRIP (Santa, sc-365383), anti-phospho ATR (S428) (Cell Signaling Technology, 2853), and anti-POL II (Abcam, ab26721). We used donkey Alexa Fluor 488-conjugated secondary antibody to rabbit (Jackson Immuno Research, 711-545-152), donkey Alexa Fluor 594-conjugated secondary antibody to mouse (Jackson Immuno Research, 715-585-150), goat Dylight 350-conjugated secondary antibody to rabbit (Abbkine, A23020), FITC-conjugated secondary antibody to human (Proteintech, SA00003-12) for 1 h at room temperature after washing with PBS and mounted using Vectorshield mounting media with DAPI. To dissect the accumulation of H3K9ac and POL II on the sex chromosomes, we used NIH's Image J software to perform the quantitative analysis as previously described [29]. The signal intensity at

the origin was assigned a value of 1 to calculate the relative intensity.

Analysis of RNA-Seq data

We used published RNA-seq datasets derived from *Uhrf1* conditional knockout (cKO) spermatocytes and MII oocyte samples for differential expression analysis, respectively [27, 30]. The datasets of *Uhrf1* cKO spermatocyte and MII oocyte samples were deposited in the GEO database under accession numbers SRP201556 and NCBI SRA database with the accession number of PRJNA659887, respectively. To identify all the transcripts, we used Tophat2 and Cufflinks to assemble the sequencing reads based on the UCSC MM10 mouse genome. Differential expression analysis was performed using the DEGseq with R. The differentially expressed genes were set with a threshold of P -value < 0.001 and fold change ≥ 2 .

RNA isolation and quantitative RT-PCR assay

Total RNA was extracted from the testes using TRIzol reagent. The concentration and purity of RNA were determined by measuring the absorbance at 260/280 nm. Total RNA (1 μ g) was reverse transcribed using a high-capacity cDNA reverse transcription kit (Vazyme) according to the manufacturer's instructions. The cDNA was subjected to real-time PCR using the SYBR qPCR master mix (Vazyme). RT-qPCR was performed on a LightCycler@96 Real-Time PCR system (Roche) according to the manufacturer's instructions. The primers used are listed in [Supplementary Table S1](#). Relative gene expression was quantified using the comparative cycle threshold method, with *Arbp* expression used for normalization.

Immunoprecipitation

Freshly isolated testes from the indicated genotypes were dissected and lysed in IP buffer (20 mM HEPES, 150 mM NaCl, 2 mM magnesium acetate, 0.2% NP-40, 1 mM DTT, pH = 7.3), clarified by centrifugation at 12 000 \times g, and then precleared with protein A beads (Bio-Rad, 161-4 013). The lysate was incubated with primary antibodies overnight at 4 $^{\circ}$ C on a rotator and conjugated with protein A beads. The beads were washed with IP buffer and then boiled in 2 \times SDS loading buffer for western blot analysis.

In vitro co-immunoprecipitation

Full-length and partial *Uhrf1* cDNA fragments were cloned into the p-CMV vector encoding a FLAG-tag. BRCA1 cDNA fragments were cloned into a p-CMV vector encoding an MYC-tag. HEK293T cells (obtained from the Stem Cell Bank of Chinese Academic Science) were transfected with the indicated plasmids using Lipofectamine 2000 (Life Technologies). Immunoprecipitation was performed after 48 h. FLAG-tagged or MYC-tagged proteins were detected by western blotting using anti-FLAG antibody (1:1 000; 20543-I-AP, Protein Tech) and anti-MYC antibody (1:10 000; 60003-2-Ig, Protein Tech).

Immunoblotting

Tissues were rinsed with PBS and lysed in cold CHAPS lysis buffer supplemented with phosphatase and protease inhibitor cocktail tablets. Tissue lysates were rotated at 4 $^{\circ}$ C for 15 min and centrifuged at 9000 rpm for 15 min at 4 $^{\circ}$ C. Protein concentration was then determined using the bicinchoninic acid (BCA) assay. Proteins (20 μ g) were separated

by sodium dodecylsulfate-polyacrylamide gel electrophoresis (SDS-PAGE) on 10% resolving gels. Protein loading was verified by blotting for α -tubulin as indicated.

Statistical analysis

All data are reported as the mean \pm SD, unless otherwise noted in the figure legends. Significance was tested using the two-tailed unpaired Student t -test ($*P < 0.05$, $**P < 0.01$, $***P < 0.001$) using Excel or Prism software.

Results

Loss of UHRF1 in male germline results in meiotic arrest and mid-to-late pachytene cells elimination

Since our previous study has reported that UHRF1 exhibits a dynamic nuclear-cytoplasmic translocation that translocates from the cytoplasm to the nucleus during meiotic prophase I [25], we further examined the localization of UHRF1 during the pachytene stage to gain a better understanding of UHRF1 in male meiosis. In control pachynema (*Stra8-Cre; Uhrf1^{+/lox}*), UHRF1 was detected in the nucleus at early pachynema and localized in the chromatin of both sex chromosomes and autosomes ([Figure 1A](#)). From early pachynema to late pachynema, the intensity of the UHRF1 signal increased and throughout the nucleus ([Figure 1A–C](#)). Interestingly, we noticed a distinguishable accumulation of UHRF1 signal at the centromeric ends of chromosomes from the mid-pachytene stage, including the centromeric end of the X chromosome ([Figure 1A–C](#) in the right panel). Because male germline-specific knockout *Uhrf1* (*Stra8-Cre* induced) in mice led to spermatocytes arrested at the pachytene stage [25, 27], we wanted to decipher the function of UHRF1 in meiotic prophase I. We first confirmed that UHRF1 signal was absent in *Stra8-Cre; Uhrf1^{lox/lox}* pachytene spermatocytes by immunofluorescence staining ([Figure 1D–F](#)). To systematically elucidate the function of UHRF1 during meiotic prophase I, we generated another male germline-specific *Uhrf1* knockout mouse model induced by *Ngn3-Cre* mice (designated as *Ngn3-Cre; Uhrf1^{lox/lox}*). *Ngn3-Cre* is expressed from postnatal day 7 (7 dpp) and fully disrupts protein expression at 9 dpp, while *Stra8-Cre* starts to express at 3 dpp with the peak expression from 7 dpp [31, 32]. Similar to *Stra8-Cre; Uhrf1^{lox/lox}* males, the *Ngn3-Cre; Uhrf1^{lox/lox}* males were also infertile. The testes weight of *Ngn3-Cre; Uhrf1^{lox/lox}* mice were reduced by approximately 4-fold relative to that of control mice (*Ngn3-Cre; Uhrf1^{lox/+}*) at 35 dpp, but showed no significant difference compared to *Stra8-Cre; Uhrf1^{lox/lox}* mice ([Supplementary Figure S1A](#)). Histological analysis of testes showed that spermatogenesis was blocked during meiosis, as post-meiotic germ cells were absent and the most advanced germ cells in seminiferous tubules were pachytene spermatocytes in both cKO mouse models ([Supplementary Figure S1B](#)). We then performed meiotic chromosome spreads from adult mice for further analysis. Further meiotic chromosome spread analyses revealed that the population of leptotene/zygotene spermatocytes in both *Stra8-Cre; Uhrf1^{lox/lox}* and *Ngn3-Cre; Uhrf1^{lox/lox}* mice was increased significantly compared to that in control mice. In contrast, compared to control mice, the population of pachytene spermatocytes decreased dramatically and diplotene spermatocytes were almost absent in both *Stra8-Cre; Uhrf1^{lox/lox}* and *Ngn3-Cre;*

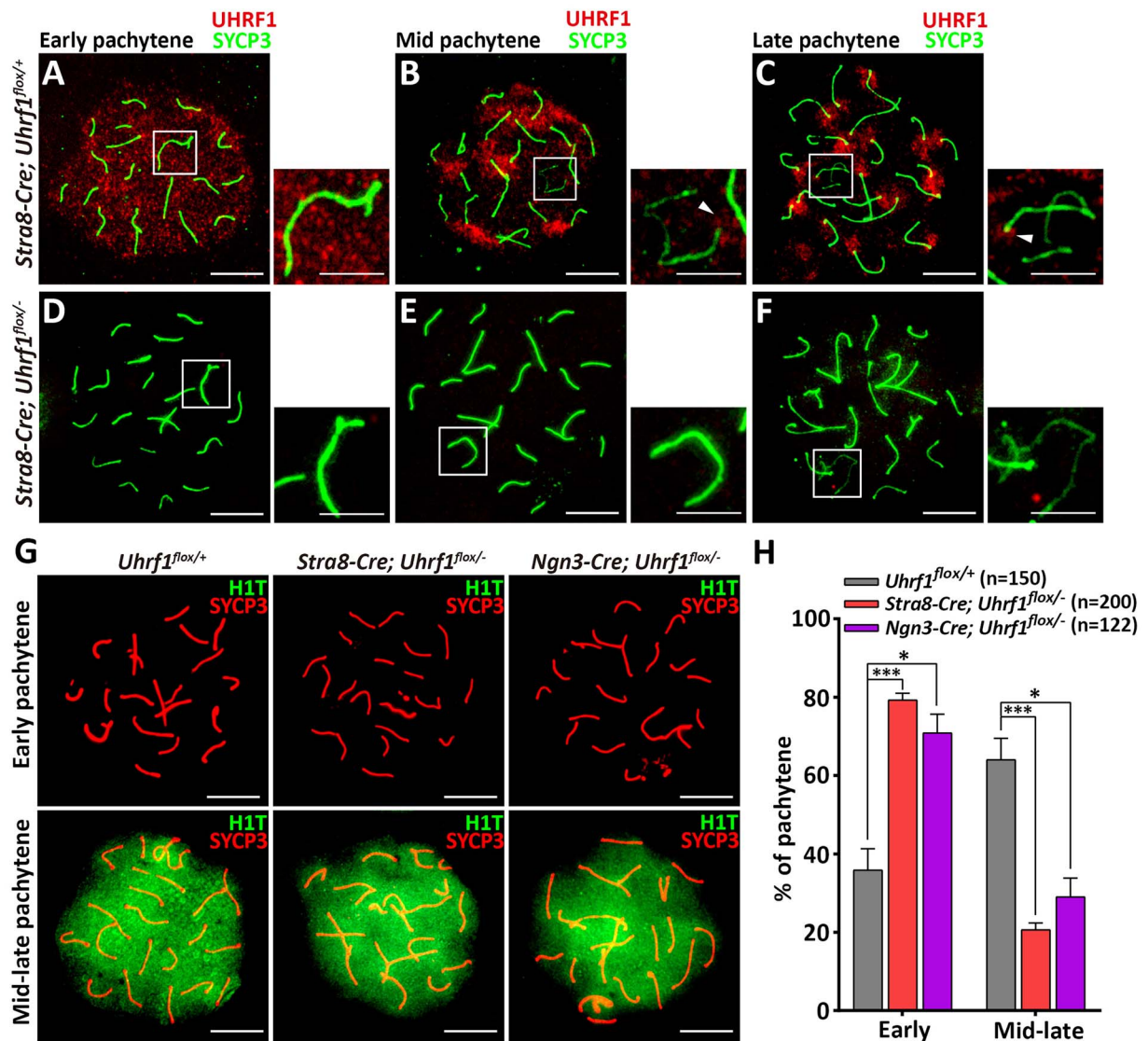


Figure 1. Meiotic deletion of UHRF1 causes the loss of mid-to-late pachytene spermatocytes. (A–F) Co-immunostaining of UHRF1 (red) and SYCP3 (green) in *Stra8-Cre; Uhrf1*^{flox/+} and *Stra8-Cre; Uhrf1*^{flox/-} pachytene spermatocytes. XY bivalent in the box is magnified in the right panels. Arrowheads indicate the centromeric end of the X chromosome. (G) Co-immunostaining of H1T (green) and SYCP3 (red) in *Uhrf1*^{flox/+}, *Stra8-Cre; Uhrf1*^{flox/-} and *Ngn3-Cre; Uhrf1*^{flox/-} pachytene spermatocytes. (H) Quantitative analysis of H1T-negative early pachytene spermatocytes and H1T-positive mid-late pachytene spermatocytes described in (G). *P*-values were derived from an unpaired Student *t*-test, **P* < 0.05 and ****P* < 0.001. Scale bars in larger panels: 10 μ m; scale bars in smaller panels: 5 μ m.

Uhrf1^{flox/-} mice (Supplementary Figure S1C–D). These results suggest that UHRF1 deficiency causes severe depletion of pachytene spermatocytes during meiosis.

To further examine the sub-stage of meiotic pachytene stage arrest, we stained meiotic chromosome spreads with antibodies against SYCP3 and a well-known mid-late pachytene marker H1T [33] (Figure 1G). We found that the ratio of H1T⁺ mid-late pachytene spermatocytes was comparable between the *Ngn3-Cre; Uhrf1*^{flox/-} and *Stra8-Cre; Uhrf1*^{flox/-} mice, but showed a significant decrease in both *Ngn3-Cre; Uhrf1*^{flox/-} and *Stra8-Cre; Uhrf1*^{flox/-} mice compared to controls (Figure 1H). Collectively, these experiments demonstrated that the *Uhrf1* germline knockout using *Stra8-Cre* and *Ngn3-Cre* shared a phenotype similar to that of meiotic arrest at the early to the mid-pachytene stage. This suggests that UHRF1-deficiency in the male germline

results in the meiotic arrest and mid-to-late pachytene cell elimination. In addition, since our previous study reported that the meiotic initiation was not affected in *Stra8-Cre; Uhrf1*^{flox/-} mice [25], we decided to focus on *Stra8-Cre; Uhrf1*^{flox/-} mice (hereafter *Uhrf1* cKO) to further study the role of UHRF1 in the meiotic process in the following study, with *Stra8-Cre; Uhrf1*^{flox/+} mice (hereafter Control) serving as controls.

UHRF1 is essential for meiotic chromosome pairing and synapsis

Since synapsis is completed at the onset of pachytene stage in male meiosis, we next investigated whether synapsis of homologous chromosomes was impaired in *Uhrf1* cKO mice to determine the cause of meiotic arrest. Synaptonemal complex protein 1 (SYCP1), the central component of the

SC, is a marker of synapsed chromosomes [34]. In contrast to SYCP1, HORMAD proteins are markers of unsynapsed or desynapsed chromosome axes, such as HORMAD1 and HORMAD2 [35–37]. Using meiotic chromosome spread assays combined with immunostaining of SYCP1 (a marker for synapsed chromosomes) and HORMAD1 (a marker for unsynapsed or desynapsed chromosomes), we found that, in the control pachytene spermatocytes, all homologous chromosomes were paired and formed synapses except for the X and Y chromosomes. The X and Y chromosomes only pair at the PAR (Figure 2A, Supplementary Figure S2A). However, after examining approximately 200 control and *Uhrf1* cKO pachytene spermatocytes, we observed severe synapsis defects in *Uhrf1* cKO spermatocytes (Figure 2B–E). Strikingly, the ratio of fully homologous chromosome synapsis was significantly decreased in *Uhrf1* cKO spermatocytes compared to control spermatocytes (Figure 2E: ~36.5% in *Uhrf1* cKO versus ~89.5% in control). In addition, we found that the majority of aberrant synapsis occurs on X and Y chromosomes, as two types of X-Y synapsis defects were revealed in *Uhrf1* cKO pachytene spermatocytes (Figure 2B and C). The main defect in *Uhrf1* cKO cells was the separated X and Y chromosomes without PAR synapsis, while the autosomes showed full synapsis (Figure 2B and Supplementary Figure S2B). The ratio of unpaired X and Y chromosomes was significantly higher in *Uhrf1* cKO pachytene cells than in controls (Figure 2E: ~36.4% in *Uhrf1* cKO versus ~6% in control). We also observed a type of synaptic defect in *Uhrf1* cKO cells characterized by the mislocalization of SYCP1 to unsynapsed axes of sex chromosomes (Figure 2C). This defect has been reported in spermatocytes with MSCI-associated gene mutations, such as *Raptor* and *Setdb1* [38, 39]. Similarly, we observed that HORMAD1 failed to accumulate over the entire length of the unsynapsed sex chromosome axes in *Uhrf1* cKOs (Supplementary Figure S2D). The ratio of SYCP1 mislocalization was significantly increased in *Uhrf1* cKO pachytene cells compared to that in controls (Figure 2E: ~8.6% in *Uhrf1* cKO versus ~3% in control). In addition to sex chromosome synapsis defects, autosome unsynapsis also occurred in *Uhrf1* cKO pachytene spermatocytes, and the frequency was significantly higher than in controls (Figure 2D and E and Supplementary Figure S2C: ~18.5% versus ~1.5%). Of note, we found a fraction of autosome-unsynapsed *Uhrf1* cKO pachytene spermatocytes exhibiting sex chromosome unsynapsis (Figure 2E: ~10.9% in *Uhrf1* cKO versus 0% in control). These data suggest that UHRF1 is required for both autosome synapsis and sex chromosome pairing.

Proper epigenetic modifications (i.e., histone H3K9 methylation) at pericentric heterochromatin (PCH) during the leptotene stage is required for subsequent homologous pairing [40], so we then examined the H3K9me3 expression in leptotene and zygotene spermatocytes of control and *Uhrf1* cKO males. Unlike the characteristic PCH enrichment of H3K9me3 in control males, *Uhrf1* cKO males exhibited a diffuse pattern of H3K9me3 distribution during the leptotene and zygotene stages (Supplementary Figure S3A–D). In particular, we observed a PCH clustering defect with H3K9me3 signals failing to fully cover the centromeres (marked by CREST) at the zygotene stage in *Uhrf1* cKO spermatocytes (Supplementary Figure S3D). This result implies defective constraining movement of chromosomes, thereby impairing homologous pairing in *Uhrf1* cKO spermatocytes. Likewise, a

recent study reported that UHRF1 promotes PCH clustering during meiosis [26]. Moreover, the intensity of H3K9me3 signal on sex chromosomes was obviously decreased in *Uhrf1* cKO spermatocytes at the early pachytene stage (Supplementary Figure S3E and F). Altogether, our data indicate that UHRF1 is essential for proper synapsis in male meiosis.

UHRF1 is required for the removal of γ H2AX from autosomes

Under normal conditions, asynapsed chromosomes trigger MSUC in male meiosis [5, 41]. Upon synapsis of autosomes complete at the onset of the pachytene stage, DDR factors (such as BRCA1, ATR, γ H2AX, etc.) diminish from autosomes and only accumulate on sex chromosomes to establish MSCI [15, 16, 42]. To assess whether the synaptic defects are associated with MSUC in *Uhrf1* cKO pachytene spermatocytes, we performed meiotic chromosome spreads using antibodies against SYCP3 and γ H2AX to examine the DDR signals in pachytene spermatocytes. The results showed that, in ~85.2% control pachynema, the γ H2AX signal was localized in the XY body (Figure 3A, column 1). In contrast, in only ~14.7% of *Uhrf1* cKO pachynema, the γ H2AX signal was properly present in the XY body (Figure 3A, column 1), suggesting that the removal of γ H2AX from autosomes was significantly impaired in a large percentage of *Uhrf1* cKO pachytene spermatocytes. In particular, we defined three types of abnormal γ H2AX accumulation patterns according to γ H2AX mislocalization. Type I was the unsynapsed autosome-induced γ H2AX retention at the autosome axes, which was observed in ~16.1% *Uhrf1* cKO pachynema, while only ~2.8% in control pachynema (Figure 3A, column 2). Moreover, we observed retained γ H2AX signals in some synapsed autosomes in ~18.6% *Uhrf1* cKO pachynema, defined as type II, which was only found in ~1.7% control pachynema (Figure 3A, column 3). Normally, the X-Y chromosomes are covered by γ H2AX signals and form an XY body distinct from autosomes during the pachytene stage. However, we found that in ~50.6% of *Uhrf1* cKO pachynema, the XY body tended to include autosomes, defined as type III, which was significantly higher than ~10.3% in control pachynema (Figure 3A, column 4). Furthermore, we examined the localization of MDC1 (a γ H2AX-binding protein that mediates the chromosome-wide spreading of γ H2AX) [13] on the XY body of *Uhrf1* cKO pachynema. We observed mislocalization of MDC1 in *Uhrf1* cKO pachynema, similar to γ H2AX in *Uhrf1* cKO pachynema (Supplementary Figure S4A–D). Together, these results indicate that UHRF1 is required for γ H2AX removal from autosomes and is associated with MSUC response during meiosis.

Failure in silencing of XY-linked genes in UHRF1-deficient pachytene spermatocytes

Since a close connection can be observed between the XY body formation and MSCI [43], we next examined whether the deletion of *Uhrf1* disrupts XY chromosome silencing in pachytene spermatocytes. To this end, we first examined the status of histone H3 acetylated at lysine9 (H3K9ac), a histone modification associated with transcriptionally active chromatin. H3K9ac localizes in the autosomes and is excluded from the XY body during the mid-late pachytene stage [44]. As expected, H3K9ac localizes in the autosomes of both

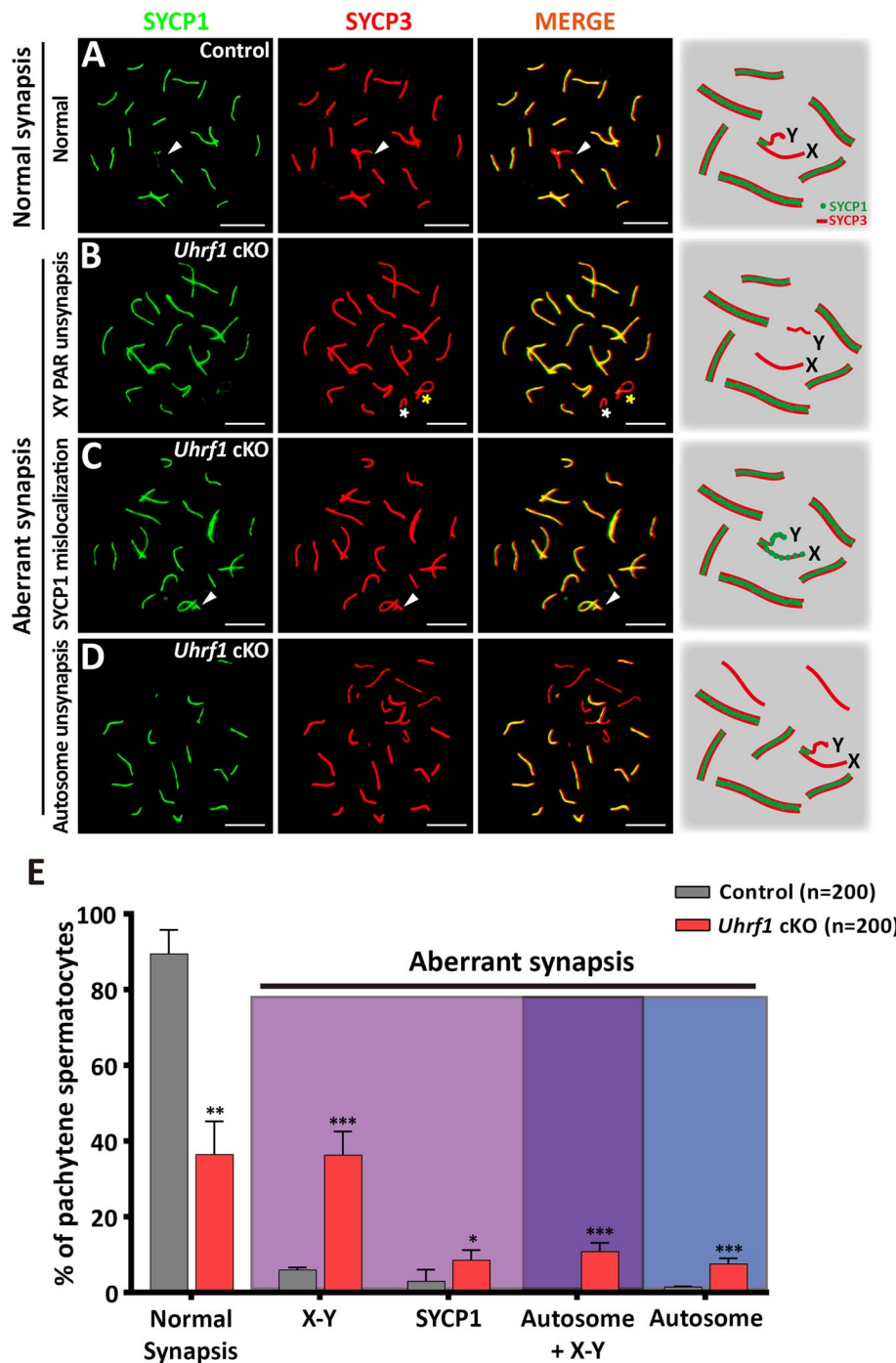


Figure 2. Defective synapsis in UHRF1-deficient pachytene spermatocytes. (A–D) Chromosome spread from control and *Uhrf1* cKO pachytene spermatocytes immunostained by SYCP1 (green) and SYCP3 (red) antibodies. SYCP1 and SYCP3 mark central and lateral elements of the synaptonemal complex, respectively. The right panels are the schematic diagram for the different types of defects in sex chromosomes and autosome synapsis. (A) Normal synapsis was characterized by co-localization of SYCP1 and SYCP3 at all autosomes except sex chromosomes. Arrowheads indicate the sex chromosomes. (B) XY PAR unsynapsis defect was characterized by unpaired X and Y chromosomes. Yellow and white asterisks indicate unpaired X and Y chromosomes, separately. (C) SYCP1 mislocalization defect was characterized by SYCP1 aberrantly localized in the nonhomologous X and Y axes. Arrowheads indicate X and Y chromosomes. (D) Autosome unsynapsis defect was characterized by SYCP1 signals lost on partial autosomes. Scale bar: 10 μ m. (E) Histogram showing the quantitative analysis of the UHRF1-deficient spermatocytes with aberrant XY chromosomes or autosomes synapsis. * $P < 0.05$; ** $P < 0.01$; *** $P < 0.001$.

control and *Uhrf1* cKO pachytene spermatocytes. Surprisingly, H3K9Ac was also detectable in the sex chromosomes of *Uhrf1* cKO pachytene spermatocytes (Figure 4A and B). Quantitative analysis revealed that pachytene spermatocytes

with H3K9Ac signal enriched on the sex chromosomes significantly increased in *Uhrf1* cKO testes compared to controls (Figure 4C: ~65.4% versus ~10.9%). Similarly, RNA polymerase II (Pol-II) was largely excluded from

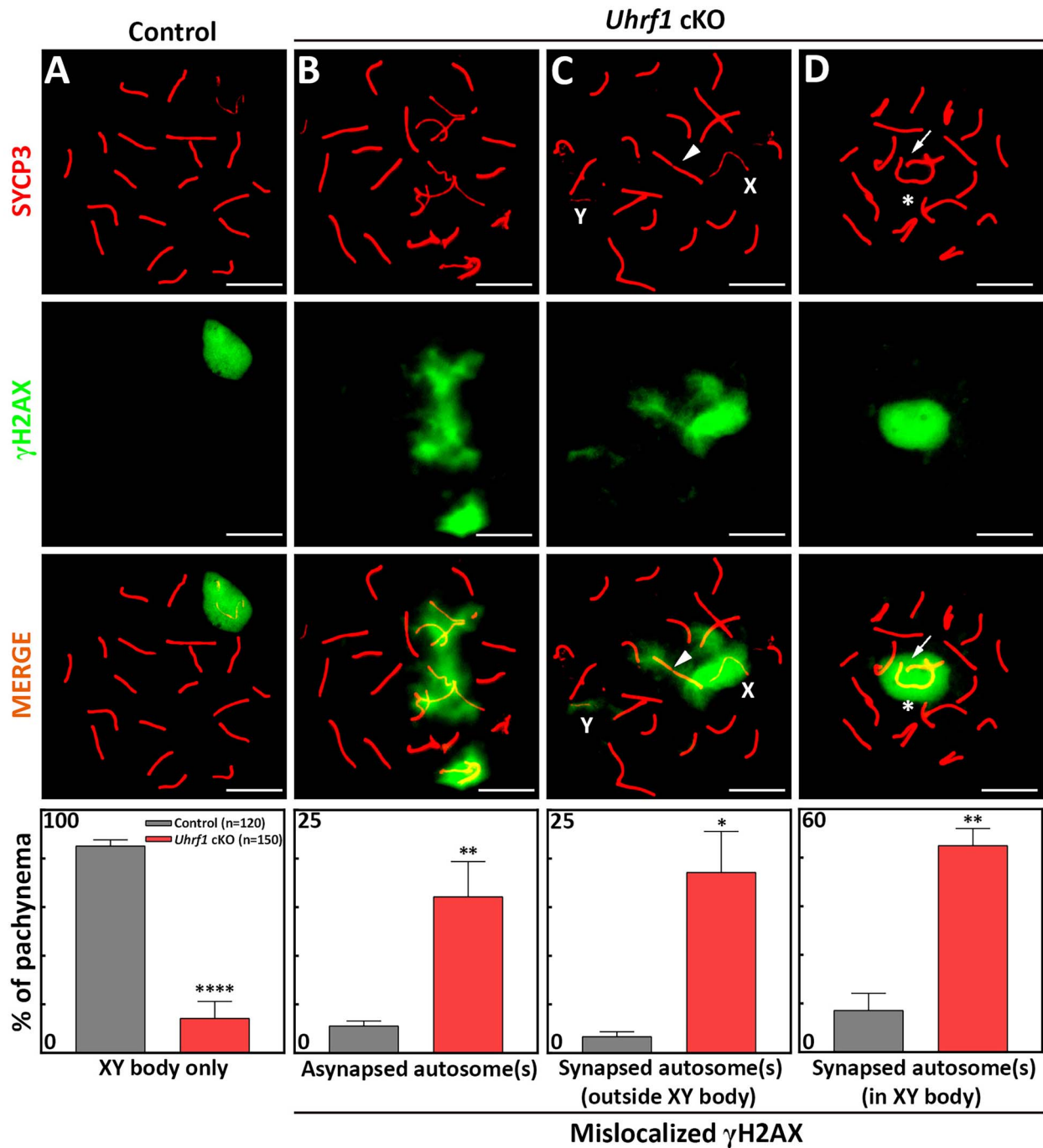


Figure 3. The localization of γ H2AX on the XY body was disturbed in UHRF1-deficient pachytene spermatocytes. (A–D) Co-immunostaining of γ H2AX (green) and SYCP3 (red) in control and *Uhrf1* cKO pachytene spermatocytes. In most of pachytene cells from the control testes, the γ H2AX signal was confined to the XY body that includes only sex chromosomes (A). In contrast, the removal of γ H2AX from autosomes was failed in *Uhrf1* cKO pachytene spermatocytes, and three types of abnormal distribution patterns of γ H2AX were observed in (B–D). The first type is the mislocalization of γ H2AX on asynapsed autosome(s) (B). The second type is the mislocalization of γ H2AX on synapsed autosome(s) (C). Arrowhead indicates the synapsed autosome. In the third type, we observed that the synapsed autosome(s) mislocalized into the position of XY body (D). Arrow indicates the autosome inside XY body, and an asterisk indicates the sex chromosome. The bottom panels in (A–D) are the quantitative analysis of the three types of γ H2AX signal distribution at the pachytene stage, respectively. * $P \leq 0.05$; ** $P \leq 0.01$; **** $P \leq 0.001$. Scale bars: 10 μ m.

the sex chromosomes in control pachytene spermatocytes, but showed an intense signal on the sex chromosomes of *Uhrf1* cKO pachytene spermatocytes (Figure 4D and E). Population analysis showed that the pachytene spermatocytes

with Pol-II signal enriched on the sex chromosomes significantly increased in *Uhrf1* cKO testes compared to controls (Figure 4F: ~67.6% versus ~11.8%). Collectively, these results suggest that UHRF1 is required for establishing MSC1.

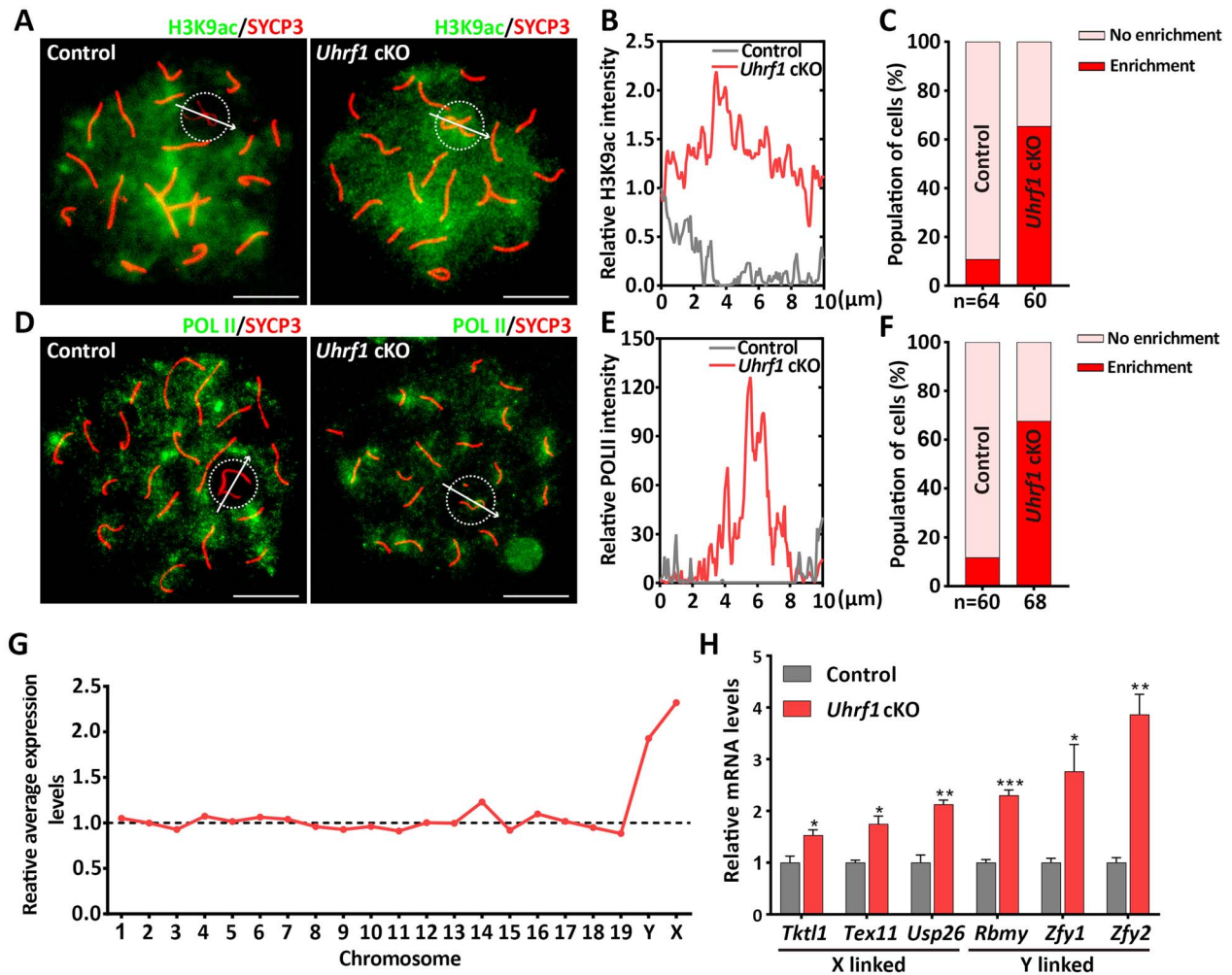


Figure 4. UHRF1 deficiency causes defective MSCI in male meiosis. (A) Pachytene spermatocytes from control and *Uhrf1* cKO immunostained by SYCP3 (red) and H3K9ac (green). Dotted circles: sex chromosomes. The indicated paths of arrows are used for the quantitative analysis of relative immunostaining intensity. Scale bars: 10 μ m. (B) Plot profiles of relative immunostaining intensity of H3K9ac in (A). (C) Population analysis of nuclei with H3K9Ac enrichment on the sex chromosomes at the pachytene stage. (D) Pachytene spermatocytes from control and *Uhrf1* cKO immunostained by SYCP3 (red) and POL II (green). Dotted circles: sex chromosomes. The indicated paths of arrows are used for the quantitative analysis of relative immunostaining intensity. Scale bars: 10 μ m. (E) Plot profiles of relative immunostaining intensity of POL II in (D). (F) Population analysis of nuclei with POL II enrichment on the sex chromosomes at the pachytene stage. (G) Relative average gene expression levels in control versus *Uhrf1* cKO mice for each individual chromosome. (H) Relative expression levels of representative X- and Y-linked genes from control and *Uhrf1* cKO testes at 18.5dpp determined by RT-qPCR (n = 3). *Arbp* mRNA expression levels were used as the loading control. * $P \leq 0.05$; ** $P \leq 0.01$; *** $P \leq 0.001$.

To further determine the role of UHRF1 in the transcriptional repression of XY-linked gene expression, we analyzed recently published RNA-Seq data of isolated spermatocytes (leptonema/zygotene and pachytene) from *Stra8-Cre; Uhrf1^{fl/fl}* and control mice by Pan et al. [27]. Interestingly, the average gene expression levels were decreased in both autosomes and sex chromosomes in *Uhrf1* cKO leptonema/zygonema (Supplementary Figure S5A), whereas the XY-linked genes were de-repressed and upregulated in *Uhrf1* cKO pachynema compared to controls (Supplementary Figure S5B). We then calculated the expression levels between the pachytene and leptotene/zygotene stages. As expected, the average expression levels of XY-linked genes in *Uhrf1* cKO pachytene were specifically upregulated compared to controls (Figure 4G). In addition, an elevation of median XY-linked gene expression was not observed in our published *Uhrf1* cKO MII oocytes RNA-seq datasets [30], suggesting that it was a pachytene-specific feature. (Supplementary Figure S5C). We next validated RNA-seq transcriptome profiles by RT-qPCR using RNA isolated

from control and *Uhrf1* cKO testes at 18.5 dpp, when MSCI was already established (Figure 4H). Notably, the expression levels of these XY-linked genes remained unchanged in *Uhrf1* cKO testes at 12.5 dpp which time point is the most advanced germ cell types are zygonema (Supplementary Figure S5D). Together, these data indicate that UHRF1 is essential for the repression of XY-linked gene expression in pachytene spermatocytes.

UHRF1 associates with DDR pathway and is required for epigenetic remodeling of the sex chromosomes

Mechanistically, the DDR pathway is essential for the establishment of MSCI [45]. BRCA1 is located on the XY axes and acts as a meiotic silencing sensor in response to the asynapsis at the beginning of the pachytene stage, after which various DDR factors such as TOPBP1 and ATR were recruited and amplified along the axes to mediate genetic

inactivation (Figure 5A). It has been reported that UHRF1 is associated with the DDR pathway during DSB repair in somatic cells [46]; however, whether UHRF1 is involved in the DDR pathway-mediated MSCI in male meiosis is unknown. To determine whether UHRF1 is related to the DDR pathway during MSCI, we first examined the localization of BRCA1 and ATR in control and *Uhrf1* cKO pachytene spermatocytes. Surprisingly, although the localization of BRCA1 was unchanged in *Uhrf1* cKO pachytene spermatocytes compared to that in controls (Figure 5D), the localization of ATR on the XY axes was seriously affected in all *Uhrf1* cKO pachytene spermatocytes. In normal male meiosis, ATR first accumulates on the XY axes at the early pachytene stage of spermatocytes and then spreads onto the chromatin loops. In contrast, ATR signals were undetectable on the XY axes in *Uhrf1* cKO early pachytene spermatocytes (Figure 5B). In addition, ATR signals failed to spread onto the chromosome-wide domain, and only a few residual ATR signals accumulated on the partial XY axes during the mid-to-late pachytene stage (Figure 5B). Phospho-S428 ATR (p-ATR), an active form of ATR, showed a similar staining pattern to ATR, with staining failing to diffuse into the XY chromatin (Figure 5C). We also observed the retained p-ATR signals on autosomes in *Uhrf1* cKO pachytene spermatocytes (Supplementary Figure S6A). We then tested the localization of two ATR cofactors, ATRIP and TOPBP1, to the XY axes [47]. Interestingly, the XY localization of ATRIP and TOPBP1 occurred normally in *Uhrf1* cKO pachytene spermatocytes (Figure 5E and F). These data indicate that UHRF1 is important for the recruitment of ATR to sex chromosomes.

Given that FANCD2 is a sex chromosome-associated factor that regulates the histone modification of sex chromosomes during male meiosis [48] and could be recruited by UHRF1 during DDR in somatic cells [49], we next examined the impact of UHRF1 deletion on the recruitment of FANCD2 on the XY axes. The results showed that in control pachytene spermatocytes, FANCD2 signals were removed from autosomes and accumulated on the XY axes. However, in *Uhrf1* cKO pachytene spermatocytes, the sequestration of FANCD2 signals from autosomes to the XY axes was impaired, exhibiting ectopic signals on autosomes (Figure 5G), suggesting that FANCD2 could not be recruited appropriately to the sex chromosomes upon UHRF1 depletion in pachytene spermatocytes. Further, western blot quantitative analysis of these associated silencing factors revealed that ATR exhibited a significant decrease and FANCD2 appeared to decrease, but not significantly in *Uhrf1* cKO testes at 18.5 dpp (Figure 5H and I). In addition, we observed that the ATR level was not impaired in *Uhrf1* cKO testes at 8.5dpp, a time point before meiosis (Supplementary Figure S6B).

Since the XY axes localization of ATR and FANCD2 is disturbed upon UHRF1 depletion, we postulate that UHRF1 plays an essential role in DDR protein regulation in MSCI. As expected, the co-immunoprecipitation analysis demonstrated that full-length UHRF1 could pull down endogenous BRCA1 in wild-type testes at 18.5 dpp (Figure 6A and B). Although our data showed that UHRF1 could not directly interact with ATR or FANCD2, recent studies have provided evidence that BRCA1 regulates the XY axis localization of ATR and FANCD2 [48]. We further mapped the sites of interaction between UHRF1 and BRCA1 by co-immunoprecipitation in HEK293T cells co-expressing a series of tagged truncation constructs of UHRF1 with BRCA1 and found that the PHD

domain could interact with BRCA1 (Figure 6C). Altogether, we concluded that UHRF1 cooperates with BRCA1 and facilitates the recruitment of DDR factors onto sex chromosomes to establish MSCI at the pachytene stage (Figure 6D).

Discussion

It is clear that UHRF1 is essential for male meiosis and fertility, as conditional ablation of *Uhrf1* in the male germline leads to pachytene spermatocyte arrest. However, the mechanisms by which UHRF1 regulates meiosis remain unclear. Based on previous studies, UHRF1 is a key epigenetic regulator that regulates the DNA methylation as well as a transposable element (TE) repression during spermatogenesis [25, 26]. Takada et al. reported that the role of UHRF1 in maintaining DNA methylation in spermatogonia is responsible for homologous synapsis defects during meiosis [26]. However, these homologous synapsis defect-induced MUSC responses cannot perfectly explain the elimination of mid-pachytene spermatocytes with aberrant X-Y synapsis. It is possible that the activation of transposons might contribute to the defective meiotic phenotype in *Uhrf1* cKO, as we previously observed that LINE1 was activated in mutant zygotene/pachytene spermatocytes [25]. However, the LINE1 activation at these stages is insufficient to cause meiotic arrest at the pachytene stage because many piRNA pathway-associated gene knockout mice exhibit LINE1 activation during the zygotene to pachytene stage and can still pass the meiosis but arrest at the spermiogenesis, such as TDRD5 [50] and PNLDC1 [51]. In addition, the DNA demethylation-induced activation of transposons in *Uhrf1* cKO is modest and may only play a minor role in meiotic defects according to previous published studies [26, 52]. Thus, we expect that TE expression may play a minor role in the meiotic defects. In this study, we showed that UHRF1 is required for both autosome and XY chromosome synapsis, sex body formation, and XY-linked gene silencing. We further revealed that UHRF1 interacts with the BRCA1, a critical factor that recruits DDR factors to sex chromosomes and drives meiotic silencing. Defective MSCI could be responsible for the elimination of mid-pachytene spermatocytes in *Uhrf1* cKO males and trigger meiotic checkpoints at the mid-pachytene stage.

One of the critical findings of this study was the defective synapsis in *Uhrf1* cKO spermatocytes. Interestingly, this phenotype was observed in both the autosomes and sex chromosomes. Previous studies have demonstrated that meiotic silencing is triggered on the unsynapsed chromosomes, termed MSUC [53]. Typically, this mechanism properly silences most of the genes on nonhomologous X-Y chromosomes in male meiosis. The unsynapsis of the PAR phenotype we observed in the current study is a typical phenotype in which, like in other meiotic mutants [34, 38, 54, 55], a relatively short length of the X-Y PAR may contribute to this synapsis defect that occurs frequently. It is noteworthy that the PAR phenotype is unlikely to effectively lead to the failure of MSCI but could cause segregation defects and thus induce apoptosis at the anaphase I stage [56–58]. Therefore, we propose that the PAR phenotype may not account for the elimination of pachytene spermatocytes in our *Uhrf1* cKO mouse model. In contrast to PAR unsynapsis, MSUC induced by extensive meiotic asynapsis in autosomes is harmful, activating the asynapsis checkpoint and inducing apoptosis during the

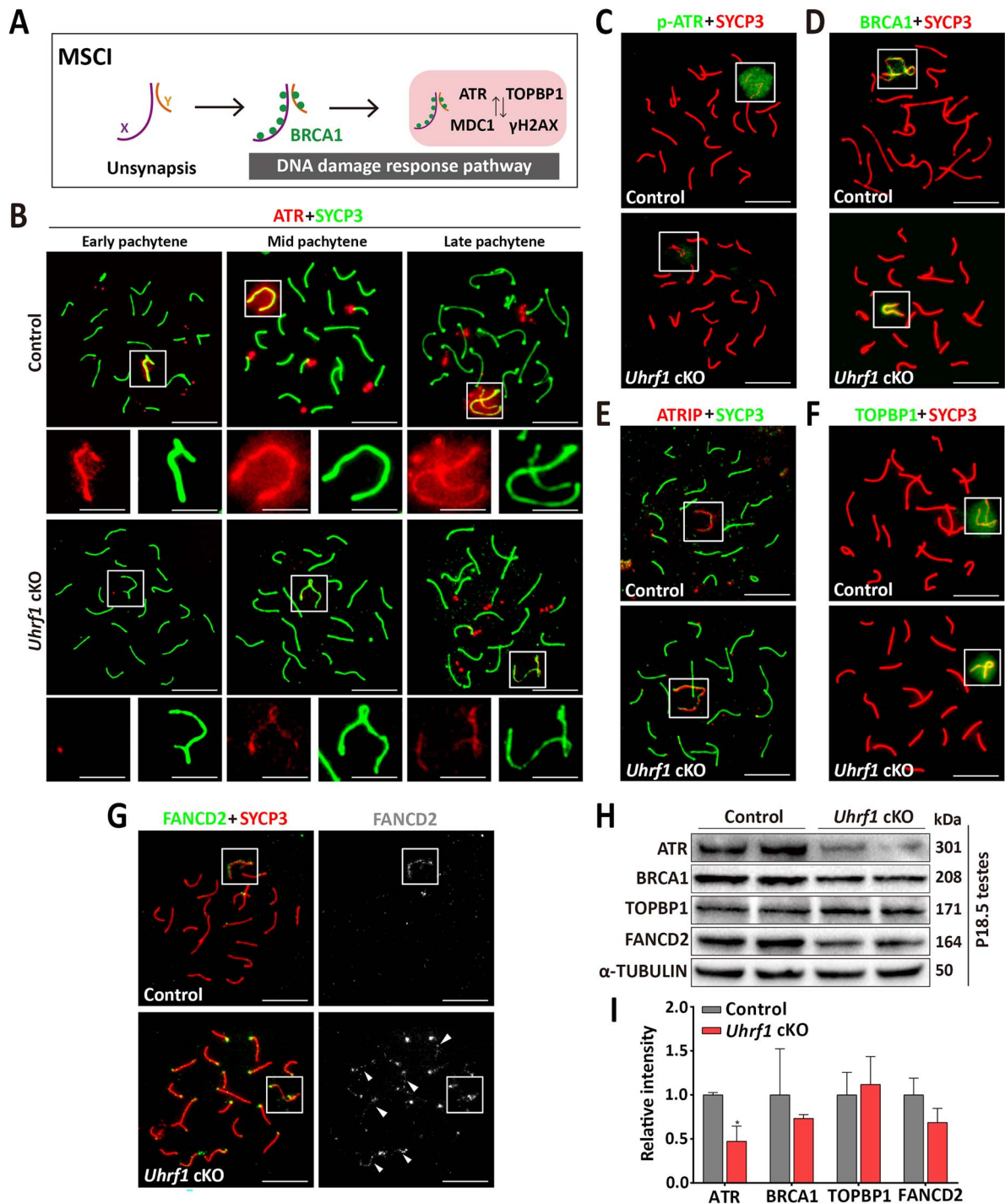


Figure 5. UHRF1 is required for the recruitment of DNA damage response factors to sex chromosomes. (A) Schematic of the DNA damage response (DDR) pathway in MSCI. (B) Early, mid-, and late pachytene from control and *Uhrf1* cKO testes immunostained by antibodies against SYCP3 (green) and ATR (red). Rectangles indicate the sex chromosomes. Scale bars: 10 μ m (on top) and 5 μ m (below). (C) Immunostaining of pachytene spermatocytes chromosome spread from control and *Uhrf1* cKO testes using antibodies against SYCP3 (red) with p-ATR (green). Rectangles indicate the sex chromosomes. Scale bars: 10 μ m. (D) Immunostaining of pachytene spermatocytes chromosome spread from control and *Uhrf1* cKO testes using antibodies against SYCP3 (red) with BRCA1 (green). Rectangles indicate the sex chromosomes. Scale bars: 10 μ m. (E) Immunostaining of pachytene spermatocytes chromosome spread from control and *Uhrf1* cKO testes using antibodies against SYCP3 (green) with ATRIP (red). Rectangles indicate the sex chromosomes. Scale bars: 10 μ m. (F) Immunostaining of pachytene spermatocytes chromosome spread from control and *Uhrf1* cKO testes using antibodies against SYCP3 (red) with TOPBP1 (green). Rectangles indicate the sex chromosomes. Scale bars: 10 μ m. (G) Immunostaining of spermatocytes chromosome spread from control and *Uhrf1* cKO testes using antibodies against SYCP3 (red) and FANCD2 (green). Arrowheads indicate ectopic foci on autosomes. Scale bars: 10 μ m. (H–I) Western blot analysis and quantification of meiotic silencing associated proteins in control and *Uhrf1* cKO testes at 18.5 dpp. Protein lysates were derived from two independent mice per genotype. α -TUBULIN serves as a loading control. * $P \leq 0.05$.

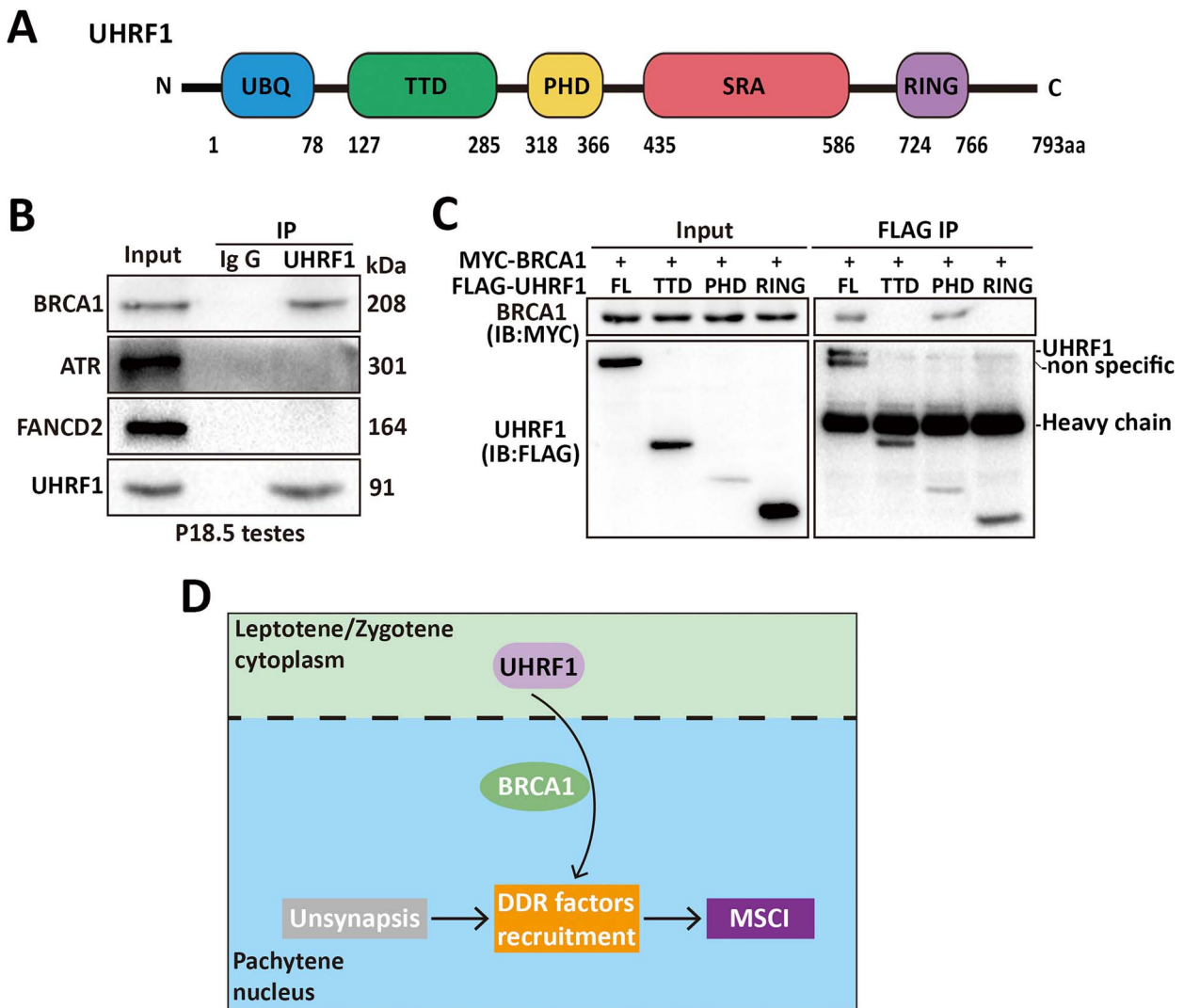


Figure 6. UHRF1 physically interacts with BRCA1 in testes. (A) The schematic illustration of UHRF1 domains. (B) Immunoprecipitation using UHRF1 or normal IgG antibodies followed by immunoblot analysis. Protein lysates were derived from control and *Uhrf1* cKO testes at 18.5 dpp. (C) FLAG-tagged UHRF1 fragments were co-transfected with MYC-BRCA1 in HEK 293 T cells. Lysates were immunoprecipitated with anti-FLAG antibodies, and the immunoprecipitated protein complex was then examined by immunoblot analysis. (D) The hypothetical model of UHRF1 interacts with BRCA1 and regulates the recruitment of DDR factors during the establishment of MSCI.

pachytene stage [5, 59]. Consistent with our previous study [25], we observed the defective H3K9me3 modification at the leptotene and zygotene stages of *Uhrf1* cKO spermatocytes in the current study. Considering the critical role of UHRF1 in DNA methylation, we proposed that UHRF1 may influence synapsis by regulating histone modification at pericentromeric heterochromatin in early meiotic prophase. Several studies have indicated that the defective H3K9 methylation at centromeric regions leads to autosome unsynapsis in meiotic mutations, such as *Setdb1*, *Suv39b1*, and *Suv39b2* [38, 60, 61]. Interestingly, a recent study provided evidence that UHRF1 and DNMT1 are required to maintain DNA methylation established in pre-meiotic spermatogonia, which is essential for pairing homologous chromosomes in the early stages of meiotic prophase [26].

The initiation of meiotic silencing on unsynapsed chromosomes requires DDR factors, such as γ H2AX which is a key factor in MSCI. Remarkably, we observed that a large proportion of *Uhrf1* cKO pachytene spermatocytes exhibited

retained γ H2AX signals on autosomes and the ectopic retention of γ H2AX signals appeared on both synapsed and asynapsed autosomes of *Uhrf1* cKO pachytene spermatocytes. In addition, we and Pan et al. previously used γ H2AX as a DSB marker to study the DSB repair defects in *Uhrf1* cKO mice [25, 27]. Notably, γ H2AX is also a marker of unsynapsed chromosomes; unsynapsed induced H2AX phosphorylation is catalyzed by the DDR factor ATR. In the current study, we carefully analyzed the abnormal localization of γ H2AX at the pachytene stage to mark the unsynapsed autosomes and XY body, which did not overlap with the previous work. Our data suggest that autosomal p-ATR retention is likely to contribute to H2AX phosphorylation on autosomes in *Uhrf1* cKO spermatocytes. A new model of MSCI generated in a recent study proposed that the DDR factors physically sequestered from autosomes to the sex chromosomes at the onset of MSCI during the early pachytene stage is a checkpoint of meiosis progression [42]. Alternatively, previous studies have revealed that the retention of DDR signals on

autosomes is largely independent of DSB repair [62–63]. In light of our results, this model may explain the massive loss of mid- to late-pachytene spermatocytes in *Uhrf1* cKO males.

Normally, the XY body formation process is critical for MSCI, during which a physically isolated and bounded compartment is formed in the pachytene nucleus [65–67]. Several studies have shown that the meiotic deletion of MSCI-associated factors leads to the failure of XY body formation [7, 16, 54, 68]. In the current study, we first identified that UHRF1 participates in proper XY body formation. The ectopic localization of autosomes on sex bodies is likely a consequence of improper sex body formation. It has been demonstrated that the amounts of DDR factors in normal pachytene spermatocytes are fixed [5]; thus, we speculate that there may exist a threshold for DDR factors on XY axes to ensure the formation of the sex body, and excessive consumption of DDR factors on autosomes leads to defective XY body formation. Furthermore, the failure of sex body formation leads to MSCI failure and derepression of XY-linked genes, which is proposed to be deleterious for pachytene spermatocytes [69–71]. However, another view is that derepression of sex-linked genes is unlikely sufficient to induce pachytene arrest [72]. Thus, further investigation is necessary to elucidate the mechanism.

How does UHRF1 regulate MSCI, or whether UHRF1 has a direct role in the MSCI regulation remains to be further determined. It is noteworthy that we detected a direct endogenous interaction between UHRF1 and BRCA1, one of the earliest DDR factors in MSCI initiation. Although the *Uhrf1* cKO mice exhibited normal accumulation of BRCA1, it is possible that UHRF1 plays a critical role downstream of BRCA1. This hypothesis is supported by previous studies showing that UHRF1 is recruited to DSB sites by BRCA1 in somatic cells [21]. Our data also revealed that UHRF1 deficiency led to incomplete recruitment of DDR factors on the sex chromosomes, such as ATR and FANCD2. In addition, ATR signals failed to diffuse from the axial elements to the XY chromatin in the absence of UHRF1. Normally, ATR is required for the proper H2AX phosphorylation on sex chromosomes [16], while recent studies have provided evidence that ATR diffusion into XY chromatin is not essential for H2AX phosphorylation [47, 73], which is consistent with our observations in this study. Intriguingly, ATR was demonstrated to regulate FANCD2 monoubiquitination and FANCD2 foci formation in somatic cells [74]. Thus, the defective localization of ATR in *Uhrf1* cKO spermatocytes may contribute to the failure of FANCD2 signal amplification on the sex chromosome. It is clear that BRCA1 is required for the recruitment of ATR on the sex chromosomes; therefore, we proposed a potential role of UHRF1 in facilitating this BRCA1-dependent manner.

In summary, our current findings suggest a novel role of UHRF1 in the regulation of the DDR pathway and meiotic silencing in mammalian spermatogenesis. Meiotic mutation of *Uhrf1* leads to the activation of the MSCI checkpoint, which triggers complete meiotic arrest and cell elimination. In comparison to the previous published researches, new information provided by the current study reveals a novel role of UHRF1 in male meiosis, which will help us better understand the phenotypes caused by UHRF1 deletion in male germ cells.

Data availability

All data needed to evaluate the conclusions in the paper are present in the article and/or the Supplementary Materials. All other supporting data of this study are available from the corresponding author upon reasonable request.

Supplementary material

Supplementary material is available at *BIOLRE* online.

Authors' contributions

M.X. and S.Y. designed this study. M.X., S.Z., and S.F. performed most of the bench experiments, Y.G. performed analysis for RNA-Seq data. J.L., Y.W., and J.D. performed some of the experiments. M.X., and S.Z. wrote the manuscript. S.Y. revised the manuscript and supervised the project. All authors read and approved the manuscript.

Conflict of interest

The authors declare that they have no conflict of interest.

References

- Zickler D, Kleckner N. A few of our favorite things: pairing, the bouquet, crossover interference and evolution of meiosis. *Semin Cell Dev Biol* 2016; 54:135–148.
- Moore DP, Orr-Weaver TL. Chromosome segregation during meiosis: building an unambivalent bivalent. *Curr Top Dev Biol* 1998; 37:263–299.
- Turner JM. Meiotic sex chromosome inactivation. *Development* 2007; 134:1823–1831.
- Cloutier JM, Mahadevaiah SK, Ellnati E, Nussenzweig A, Tóth A, Turner JM. Histone H2AFX links meiotic chromosome asynapsis to prophase I oocyte loss in mammals. *PLoS Genet* 2015; 11:e1005462.
- Mahadevaiah SK, Bourc'his D, de Rooij DG, Bestor TH, Turner JM, Burgoyne PS. Extensive meiotic asynapsis in mice antagonises meiotic silencing of unsynapsed chromatin and consequently disrupts meiotic sex chromosome inactivation. *J Cell Biol* 2008; 182:263–276.
- Campbell P, Good JM, Nachman MW. Meiotic sex chromosome inactivation is disrupted in sterile hybrid male house mice. *Genetics* 2013; 193:819–828.
- Ellnati E, Russell HR, Ojarikre OA, Sangrithi M, Hirota T, de Rooij DG, McKinnon PJ, Turner JMA. DNA damage response protein TOPBP1 regulates X chromosome silencing in the mammalian germ line. *Proc Natl Acad Sci USA* 2017; 114:12536–12541.
- Schoenmakers S, Wassenaar E, van Cappellen WA, Derijck AA, de Boer P, Laven JS, Grootegoed JA, Baarends WM. Increased frequency of asynapsis and associated meiotic silencing of heterologous chromatin in the presence of irradiation-induced extra DNA double strand breaks. *Dev Biol* 2008; 317:270–281.
- Turner JM. Meiotic silencing in mammals. *Annu Rev Genet* 2015; 49:395–412.
- Turner JM, Mahadevaiah SK, Fernandez-Capetillo O, Nussenzweig A, Xu X, Deng CX, Burgoyne PS. Silencing of unsynapsed meiotic chromosomes in the mouse. *Nat Genet* 2005; 37:41–47.
- Ceccaldi R, Rondinelli B, D'Andrea AD. Repair pathway choices and consequences at the double-strand break. *Trends Cell Biol* 2016; 26:52–64.

12. Polo SE, Jackson SP. Dynamics of DNA damage response proteins at DNA breaks: a focus on protein modifications. *Genes Dev* 2011; 25:409–433.
13. Ichijima Y, Ichijima M, Lou Z, Nussenzweig A, Camerini-Otero RD, Chen J, Andreassen PR, Namekawa SH. MDC1 directs chromosome-wide silencing of the sex chromosomes in male germ cells. *Genes Dev* 2011; 25:959–971.
14. Turner JM, Aprelikova O, Xu X, Wang R, Kim S, Chandramouli GV, Barrett JC, Burgoyne PS, Deng CX. BRCA1, histone H2AX phosphorylation, and male meiotic sex chromosome inactivation. *Curr Biol* 2004; 14:2135–2142.
15. Broering TJ, Alavattam KG, Sadreyev RI, Ichijima Y, Kato Y, Hasegawa K, Camerini-Otero RD, Lee JT, Andreassen PR, Namekawa SH. BRCA1 establishes DNA damage signaling and pericentric heterochromatin of the X chromosome in male meiosis. *J Cell Biol* 2014; 205:663–675.
16. Royo H, Prosser H, Ruzankina Y, Mahadevaiah SK, Cloutier JM, Baumann M, Fukuda T, Höög C, Tóth A, de Rooij DG, Bradley A, Brown EJ *et al.* ATR acts stage specifically to regulate multiple aspects of mammalian meiotic silencing. *Genes Dev* 2013; 27:1484–1494.
17. Chen H, Ma H, Inuzuka H, Diao J, Lan F, Shi YG, Wei W, Shi Y. DNA damage regulates UHRF1 stability via the SCF(β -TrCP) E3 ligase. *Mol Cell Biol* 2013; 33:1139–1148.
18. Muto M, Fujimori A, Neno M, Daino K, Matsuda Y, Kuroiwa A, Kubo E, Kanari Y, Utsuno M, Tsuji H, Ukai H, Mita K *et al.* Isolation and characterization of a novel human radiosusceptibility gene, NP95. *Radiat Res* 2006; 166:723–733.
19. Muto M, Kanari Y, Kubo E, Takabe T, Kurihara T, Fujimori A, Tatsumi K. Targeted disruption of Np95 gene renders murine embryonic stem cells hypersensitive to DNA damaging agents and DNA replication blocks. *J Biol Chem* 2002; 277:34549–34555.
20. Tien AL, Senbanerjee S, Kulkarni A, Mudbhary R, Goudreau B, Ganesan S, Sadler KC, Ukomadu C. UHRF1 depletion causes a G2/M arrest, activation of DNA damage response and apoptosis. *Biochem J* 2011; 435:175–185.
21. Zhang H, Liu H, Chen Y, Yang X, Wang P, Liu T, Deng M, Qin B, Correia C, Lee S, Kim J, Sparks M *et al.* A cell cycle-dependent BRCA1-UHRF1 cascade regulates DNA double-strand break repair pathway choice. *Nat Commun* 2016; 7:10201.
22. Hahm JY, Kim JY, Park JW, Kang JY, Kim KB, Kim SR, Cho H, Seo SB. Methylation of UHRF1 by SET7 is essential for DNA double-strand break repair. *Nucleic Acids Res* 2019; 47:184–196.
23. Tian D, Tang J, Geng X, Li Q, Wang F, Zhao H, Narla G, Yao X, Zhang Y. Targeting UHRF1-dependent DNA repair selectively sensitizes KRAS mutant lung cancer to chemotherapy. *Cancer Lett* 2020; 493:80–90.
24. Tian Y, Paramasivam M, Ghosal G, Chen D, Shen X, Huang Y, Akhter S, Legerski R, Chen J, Seidman MM, Qin J, Li L. UHRF1 contributes to DNA damage repair as a lesion recognition factor and nuclease scaffold. *Cell Rep* 2015; 10:1957–1966.
25. Dong J, Wang X, Cao C, Wen Y, Sakashita A, Chen S, Zhang J, Zhang Y, Zhou L, Luo M, Liu M, Liao A *et al.* UHRF1 suppresses retrotransposons and cooperates with PRMT5 and PIWI proteins in male germ cells. *Nat Commun* 2019; 10:4705.
26. Takada Y, Yaman-Deveci R, Shirakawa T, Sharif J, Tomizawa S-I, Miura F, Ito T, Ono M, Nakajima K, Koseki Y, Shiotani F, Ishiguro K-I *et al.* Maintenance DNA methylation in pre-meiotic germ cells regulates meiotic prophase by facilitating homologous chromosome pairing. *Development* 2021; 148:dev194605.
27. Pan H, Jiang N, Sun S, Jiang H, Xu J, Jiang X, Gao Q, Li L, Wu H, Zheng H, Qi Q, Li T *et al.* UHRF1-repressed 5'-hydroxymethylcytosine is essential for the male meiotic prophase I. *Cell Death Dis* 2020; 11:142.
28. Alavattam KG, Abe H, Sakashita A, Namekawa SH. Chromosome spread analyses of meiotic sex chromosome inactivation. *Methods Mol Biol* 2018; 1861:113–129.
29. Sin H-S, Barski A, Zhang F, Kartashov AV, Nussenzweig A, Chen J, Andreassen PR, Namekawa SH. RNF8 regulates active epigenetic modifications and escape gene activation from inactive sex chromosomes in post-meiotic spermatids. *Genes Dev* 2012; 26:2737–2748.
30. Wu Y, Dong J, Feng S, Zhao Q, Duan P, Xiong M, Wen Y, Lv C, Wang X, Yuan S. Maternal UHRF1 is essential for transcription landscapes and repression of repetitive elements during the maternal-to-zygotic transition. *Front Cell Dev Biol* 2020; 8:610773.
31. Yoshida S, Takakura A, Ohbo K, Abe K, Wakabayashi J, Yamamoto M, Suda T, Nabeshima Y. Neurogenin3 delineates the earliest stages of spermatogenesis in the mouse testis. *Dev Biol* 2004; 269:447–458.
32. Sadate-Ngatchou PI, Payne CJ, Dearth AT, Braun RE. Cre recombinase activity specific to postnatal, premeiotic male germ cells in transgenic mice. *Genesis* 2008; 46:738–742.
33. Drabent B, Bode C, Bramlage B, Doenecke D. Expression of the mouse testicular histone gene H1t during spermatogenesis. *Histochem Cell Biol* 1996; 106:247–251.
34. de Vries FA, de Boer E, van den Bosch M, Baarends WM, Ooms M, Yuan L, Liu JG, van Zeeland AA, Heyting C, Pastink A. Mouse Sycp1 functions in synaptonemal complex assembly, meiotic recombination, and XY body formation. *Genes Dev* 2005; 19:1376–1389.
35. Fukuda T, Daniel K, Wojtasz L, Toth A, Höög C. A novel mammalian HORMA domain-containing protein, HORMAD1, preferentially associates with unsynapsed meiotic chromosomes. *Exp Cell Res* 2010; 316:158–171.
36. Wojtasz L, Daniel K, Roig I, Bolcun-Filas E, Xu H, Boonsanay V, Eckmann CR, Cooke HJ, Jasin M, Keeney S, McKay MJ, Toth A. Mouse HORMAD1 and HORMAD2, two conserved meiotic chromosomal proteins, are depleted from synapsed chromosome axes with the help of TRIP13 AAA-ATPase. *PLoS Genet* 2009; 5:e1000702.
37. Shin Y-H, Choi Y, Erdin SU, Yatsenko SA, Kloc M, Yang F, Wang PJ, Meistrich ML, Rajkovic A. Hormad1 mutation disrupts synaptonemal complex formation, recombination, and chromosome segregation in mammalian meiosis. *PLoS Genet* 2010; 6:e1001190.
38. Cheng EC, Hsieh CL, Liu N, Wang J, Zhong M, Chen T, Li E, Lin H. The essential function of SETDB1 in homologous chromosome pairing and synapsis during meiosis. *Cell Rep* 2021; 34:108575.
39. Xiong M, Zhu Z, Tian S, Zhu R, Bai S, Fu K, Davis JG, Sun Z, Baur JA, Zheng K, Ye L. Conditional ablation of in the male germline causes infertility due to meiotic arrest and impaired inactivation of sex chromosomes. *FASEB J* 2017; 31:3934–3949.
40. Takada Y, Naruse C, Costa Y, Shirakawa T, Tachibana M, Sharif J, Kezuka-Shiotani F, Kakiuchi D, Masumoto H, Shinkai Y-I, Ohbo K, Peters AHFM *et al.* HP1 γ links histone methylation marks to meiotic synapsis in mice. *Development* 2011; 138:4207–4217.
41. Turner JM, Mahadevaiah SK, Ellis PJ, Mitchell MJ, Burgoyne PS. Pachytene asynapsis drives meiotic sex chromosome inactivation and leads to substantial postmeiotic repression in spermatids. *Dev Cell* 2006; 10:521–529.
42. Abe H, Alavattam KG, Hu Y-C, Pang Q, Andreassen PR, Hegde RS, Namekawa SH. The initiation of meiotic sex chromosome inactivation sequesters DNA damage signaling from autosomes in mouse spermatogenesis. *Curr Biol* 2020; 30:408–420.
43. Yan W, McCarrey JR. Sex chromosome inactivation in the male. *Epigenetics* 2009; 4:452–456.
44. Page J, de la Fuente R, Manterola M, Parra MT, Viera A, Berríos S, Fernández-Donoso R, Rufas JS. Inactivation or non-reactivation: what accounts better for the silence of sex chromosomes during mammalian male meiosis? *Chromosoma* 2012; 121:307–326.
45. Ichijima Y, Sin HS, Namekawa SH. Sex chromosome inactivation in germ cells: emerging roles of DNA damage response pathways. *Cell Mol Life Sci* 2012; 69:2559–2572.
46. Mancini M, Magnani E, Macchi F, Bonapace IM. The multifunctionality of UHRF1: epigenome maintenance and preservation of genome integrity. *Nucleic Acids Res* 2021; 49:6053–6068.
47. Yeo AJ, Becherel OJ, Luff JE, Graham ME, Richard D, Lavin MF. Senataxin controls meiotic silencing through ATR activation and chromatin remodeling. *Cell discovery* 2015; 1:15025.

48. Alavattam KG, Kato Y, Sin H-S, Maezawa S, Kowalski IJ, Zhang F, Pang Q, Andreassen PR, Namekawa SH. Elucidation of the Fanconi anemia protein network in meiosis and its function in the regulation of histone modifications. *Cell Rep* 2016; **17**: 1141–1157.
49. Liang C-C, Zhan B, Yoshikawa Y, Haas W, Gygi SP, Cohn MA. UHRF1 is a sensor for DNA interstrand crosslinks and recruits FANCD2 to initiate the Fanconi anemia pathway. *Cell Rep* 2015; **10**:1947–1956.
50. Yabuta Y, Ohta H, Abe T, Kurimoto K, Chuma S, Saitou M. TDRD5 is required for retrotransposon silencing, chromatoid body assembly, and spermiogenesis in mice. *J Cell Biol* 2011; **192**: 781–795.
51. Ding DQ, Liu JL, Dong KZ, Midic U, Hess RA, Xie HR, Demireva EY, Chen C. PNLDC1 is essential for piRNA 3' end trimming and transposon silencing during spermatogenesis in mice. *Nat Commun* 2017; **8**:819.
52. Shirakawa T, Yaman-Deveci R, Tomizawa S-I, Kamizato Y, Nakajima K, Sone H, Sato Y, Sharif J, Yamashita A, Takada-Horisawa Y, Yoshida S, Ura K *et al.* An epigenetic switch is crucial for spermatogonia to exit the undifferentiated state toward a Kit-positive identity. *Development* 2013; **140**:3565–3576.
53. Manterola M, Page J, Vasco C, Berríos S, Parra MT, Viera A, Rufas JS, Zuccotti M, Garagna S, Fernández-Donoso R. A high incidence of meiotic silencing of unsynapsed chromatin is not associated with substantial pachytene loss in heterozygous male mice carrying multiple simple Robertsonian translocations. *PLoS Genet* 2009; **5**:e1000625.
54. Fernandez-Capetillo O, Mahadevaiah SK, Celeste A, Romanienko PJ, Camerini-Otero RD, Bonner WM, Manova K, Burgoyne P, Nussenzweig A. H2AX is required for chromatin remodeling and inactivation of sex chromosomes in male mouse meiosis. *Dev Cell* 2003; **4**:497–508.
55. Widger A, Mahadevaiah SK, Lange J, Ellnati E, Zohren J, Hirota T, Pacheco S, Maldonado-Linares A, Stanzione M, Ojarikre O, Maciulyte V, de Rooij DG *et al.* ATR is a multifunctional regulator of male mouse meiosis. *Nat Commun* 2018; **9**:2621.
56. Yang F, Gell K, van der Heijden GW, Eckardt S, Leu NA, Page DC, Benavente R, Her C, Höög C, McLaughlin KJ, Wang PJ. Meiotic failure in male mice lacking an X-linked factor. *Genes Dev* 2008; **22**:682–691.
57. Eaker S, Cobb J, Pyle A, Handel MA. Meiotic prophase abnormalities and metaphase cell death in MLH1-deficient mouse spermatocytes: insights into regulation of spermatogenic progress. *Dev Biol* 2002; **249**:85–95.
58. Li X, Nicklas RB. Mitotic forces control a cell-cycle checkpoint. *Nature* 1995; **373**:630–632.
59. de Rooij DG, de Boer P. Specific arrests of spermatogenesis in genetically modified and mutant mice. *Cytogenet Genome Res* 2003; **103**:267–276.
60. Baudat F, Imai Y, de Massy B. Meiotic recombination in mammals: localization and regulation. *Nat Rev Genet* 2013; **14**:794–806.
61. Da Ines O, White CI. Centromere associations in meiotic chromosome pairing. *Annu Rev Genet* 2015; **49**:95–114.
62. Li XC, Schimenti JC. Mouse pachytene checkpoint 2 (trip13) is required for completing meiotic recombination but not synapsis. *PLoS Genet* 2007; **3**:e130.
63. Roig I, Dowdle JA, Toth A, de Rooij DG, Jasin M, Keeney S. Mouse TRIP13/PCH2 is required for recombination and normal higher-order chromosome structure during meiosis. *PLoS Genet* 2010; **6**:e1001062.
64. Pacheco S, Marcet-Ortega M, Lange J, Jasin M, Keeney S, Roig I. The ATM signaling cascade promotes recombination-dependent pachytene arrest in mouse spermatocytes. *PLoS Genet* 2015; **11**:e1005017.
65. Handel MA. The XY body: a specialized meiotic chromatin domain. *Exp Cell Res* 2004; **296**:57–63.
66. Bellani MA, Romanienko PJ, Cairatti DA, Camerini-Otero RD. SPO11 is required for sex-body formation, and Spo11 heterozygosity rescues the prophase arrest of *Atm*^{-/-} spermatocytes. *J Cell Sci* 2005; **118**:3233–3245.
67. Alavattam KG, Maezawa S, Sakashita A, Khoury H, Barski A, Kaplan N, Namekawa SH. Attenuated chromatin compartmentalization in meiosis and its maturation in sperm development. *Nat Struct Mol Biol* 2019; **26**:175–184.
68. Hirota T, Blakeley P, Sangrithi MN, Mahadevaiah SK, Encheva V, Snijders AP, Ellnati E, Ojarikre OA, de Rooij DG, Niakan KK, Turner JMA. SETDB1 links the meiotic DNA damage response to sex chromosome silencing in mice. *Dev Cell* 2018; **47**:645–659.
69. Royo H, Polikiewicz G, Mahadevaiah SK, Prosser H, Mitchell M, Bradley A, de Rooij DG, Burgoyne PS, Turner JM. Evidence that meiotic sex chromosome inactivation is essential for male fertility. *Curr Biol* 2010; **20**:2117–2123.
70. Odorisio T, Mahadevaiah SK, McCarrey JR, Burgoyne PS. Transcriptional analysis of the candidate spermatogenesis gene *Ube1y* and of the closely related *Ube1x* shows that they are coexpressed in spermatogonia and spermatids but are repressed in pachytene spermatocytes. *Dev Biol* 1996; **180**:336–343.
71. Mahadevaiah SK, Odorisio T, Elliott DJ, Rattigan A, Szot M, Laval SH, Washburn LL, McCarrey JR, Cattanaach BM, Lovell-Badge R, Burgoyne PS. Mouse homologues of the human AZF candidate gene *RBM* are expressed in spermatogonia and spermatids, and map to a Y chromosome deletion interval associated with a high incidence of sperm abnormalities. *Hum Mol Genet* 1998; **7**: 715–727.
72. Hasegawa K, Sin H-S, Maezawa S, Broering TJ, Kartashov AV, Alavattam KG, Ichijima Y, Zhang F, Bacon WC, Greis KD, Andreassen PR, Barski A *et al.* SCML2 establishes the male germline epigenome through regulation of histone H2A ubiquitination. *Dev Cell* 2015; **32**:574–588.
73. Becherel OJ, Yeo AJ, Stellati A, Heng EYH, Luff J, Suraweera AM, Woods R, Fleming J, Carrie D, McKinney K, Xu X, Deng C *et al.* Senataxin plays an essential role with DNA damage response proteins in meiotic recombination and gene silencing. *PLoS Genet* 2013; **9**:e1003435.
74. Andreassen PR, D'Andrea AD, Taniguchi T. ATR couples FANCD2 monoubiquitination to the DNA-damage response. *Genes Dev* 2004; **18**:1958–1963.